**Notice of Violation of IEEE Publication Principles**

**"Channel Equalization and Data Detection of OVFDM under Fading Channel"**
by Yue Hu, Yafeng Wang, and Haocheng Wang
in IEEE Access, Vol 8, April 2020, pp. 77120-77130

After careful and considered review of the content and authorship of this paper by a duly constituted expert committee, this paper has been found to be in violation of IEEE's Publication Principles.

This paper contains copied content from the paper cited below. The original content was copied without attribution (including appropriate references to the original author(s) and/or paper title) and without permission.

**"Channel Equalisation and Data Detection for SEFDM Over Frequency Selective Fading Channels"**
by Baoxian Yu, Han Zhang, Xudong Hong, Changjian Guo, Alan Pak Tao Lau, Chao Lu, Xianhua Dai
in IET Communications, Vol 12, Issue 18, November 2018, pp. 2315-2323

IEEE Access
Multidisciplinary | Rapid Review | Open Access Journal

Received March 9, 2020, accepted April 5, 2020, date of publication April 27, 2020, date of current version May 7, 2020.

*Digital Object Identifier 10.1109/ACCESS.2020.2989801*

# Channel Equalization and Data Detection of OVFDM Under Fading Channel

**YUE HU, (Graduate Student Member, IEEE), YAFENG WANG, (Senior Member, IEEE), AND HAOCHENG WANG**

Key Laboratory of Universal Wireless Communication, Ministry of Education, Beijing University of Posts and Telecommunications, Beijing 100876, China

Corresponding author: Yafeng Wang (wangyf@bupt.edu.cn)

This work was supported in part by the Ministry of Education and China Mobile Joint Scientific Research Fund under Grant MCM20180201.

**ABSTRACT** Obtaining high spectral efficiency by overlapping and weighting multiplexing waveforms, OVFDM (Overlapped Frequency Division Multiplexing) system is considered to be a promising multi-carrier technology in future communication networks. Limited by the non-orthogonality between subcarriers, OVFDM systems usually use MLSD (Maximum Likelihood Sequence Detection) algorithm for decoding, which brings high computational complexity and thus limits the applying of OVFDM system in engineering. In this paper, a ZP (Zero-padding) - OVFDM architecture is proposed and the architecture can benefit from frequency diversity. Meanwhile, compared with the MLSD algorithm, the proposed MAP (Maximum A Posteriori) -based Viterbi decoding algorithm has better performance and requires much less computation by evaluating the likelihood of each detection and discarding the least possible ones based on the MAP criterion. The numerical results show that OVFDM can provide superior performance over OFDM on frequency selective fading channels.

**INDEX TERMS** Overlapped frequency division multiplexing (OVFDM), fading channel, channel equalization, inter-carrier interference (ICI), low complexity decoding algorithm.

## I. INTRODUCTION

O verlapped Frequency Division Multiplexing (OVFDM) is a communication technology based on the overlapped multiplexing principle, which provides high spectral efficiency technique [1]. Compared with Orthogonal Frequency Division Multiplexing (OFDM), OVFDM distributes subcarriers more compact in frequency domain, which leads to higher spectral efficiency [2]. Based on the above superiority, OVFDM has great application prospects in future mobile network [3], [4]. However, it suffers Inter-carrier Interference (ICI) by non-orthogonality between adjacent subcarriers. For the high spectral efficiency potential of OVFDM, we must consider the following aspects.

### A. TRANSCEIVER

OFDM benefits from the advantage of Inverse Discrete Fourier Transform (IDFT) transmitter and it is widely used in modern communication systems [5]. As pointed out in [6], IDFT is no longer suitable to generate OVFDM signals directly. However, Inverse Fractional Fourier Transform [7] shows the competence which can generate OVFDM signals. Under the constraint of the overlapped multiplexing coefficient $K$, OVFDM signals can be constructed by superposition of multiple IDFTs. Therefore, the design complexity of the IDFT-based OVFDM transceiver is acceptable in engineering applications.

### B. FADING CHANNEL

Because of the non-orthogonality between subcarriers, the OVFDM system will not use the pilot-assisted channel estimation and the typical single-tap zero-forcing (ZF) frequency domain equalizer (FDE) applied in OFDM system [8]–[10]. In [5], Weinstein and Ebert proposed a maximum likelihood sequence detection (MLSD) receiver that it uses an implicit frequency diversity to improve system performance. This equalisation method performs well when integrating with the optimal detector, but it costs too much computation.

### C. DECODING ALGORITHM

The artificial introduction of ICI in the OVFDM system makes decoding difficult. In [11], Zhao *et al.* proposed

The associate editor coordinating the review of this manuscript and approving it for publication was Cunhua Pan.

the sphere decoding (SD) [12] for Overlapped Time Division Multiplexing (OVTDM) system and achieved a good decoding effect. In general, SD algorithm requires too many calculations in the case of large symbol sizes, high noise levels or large $K$ (overlapped multiplexing coefficient), which makes it limited in practical engineering applications. Although low-complexity sliding window block decoding using bit flipping [13] effectively reduces decoding complexity and has excellent decoding performance, it has high requirements for constraint length. In [14], the multi-bit sliding stack decoding (Multi-Bit SSD) algorithm is proposed to simultaneously implement multi-bit decoding in Overlapped X Domain Multiplexing (OVXDM). However, its decoding performance is limited by the size of the sliding window. When the sliding window size is larger, the algorithm decoding performance is better, and its computational complexity is higher. Therefore, how to choose the sliding window size is a big challenge in different situations. A low complexity multiple signal joint decoding (MSJD) algorithm [15] for OVXDM is proposed for the additive white Gaussian noise (AWGN) channel and it is extended to frequency selective fading channel. To find the optimal OVXDM system performance, the key part of the algorithm is to choose the appropriate number of received signals. But how to choose the right number of received signals is a big challenge. In short, the OVFDM decoding algorithm is still the bottleneck in engineering applications.

### D. CONTRIBUTIONS

In view of the above problems, we study the transceiver design of OVFDM on the frequency selective fading channel, especially focusing on channel equalization and decoding algorithm of OVFDM. In particular, the contributions of this paper are summarized as follows.

We design a framework of OVFDM transceiver and introduce zero-padding (ZP) aided OVFDM (ZP-OVFDM) for OVFDM. Utilizing the ZP suffix, we formulate the time domain OVFDM signal into a cyclic structure at the receiver and perform channel equalization in the frequency domain. Through the mathematical analysis of OVFDM signal in fading channel, it confirms that the proposed equalization scheme benefits from the frequency diversity with ICI, which proves that OVFDM has the potential to improve system performance compared with OFDM.

The rest of this paper is organized as follows. In Section 2, we introduce the OVFDM system model, spectral efficiency, and channel model. Section 3 describes the ZP-OVFDM architecture and provides a theoretical analysis of OVFDM system in fading channel. In Section 4, we propose a new decoding scheme based on Maximum a posteriori (MAP). The simulation results are shown in Section 5, and Section 6 summarizes this article.

*Notation:* Bold italic face lower (upper) case letters denote vectors (matrices). $(\cdot)^T$, $(\cdot)^H$ and $(\cdot)^\dagger$ represent transpose, Hermitian transpose and pseudo-reverse, respectively. $[\cdot]_i$ represents the $i$-th entry of a vector, and $[\cdot]_{i,j}$ represents the $(i, j)$-th entry of a matrix. $\boldsymbol{I}_N$ is an identity matrix of size $N$. $\mathbf{0}_{p\times 1}$ and $\mathbf{1}_{p\times 1}$ represent a $p\times 1$ matrix in which all entries are zero and 1, respectively. $\mathbb{S}_P$ represents a finite set of vectors with a length of $P$ and $|\mathbb{S}_P|$ denotes its cardinality.

## II. OVFDM SYSTEM MODEL

OVFDM is an implementation of overlapped multiplexing principle in the frequency domain. Compared with OFDM, OVFDM has stronger overlapping than OFDM between subcarrier bands, which has smaller subcarrier spacing and higher spectral efficiency. It improves the spectral efficiency of system by overlapping and weighting signals. It is worth noting that OVTDM overlaps and weights the time domain waveforms to increase the transmission rate and OVFDM overlaps and weights the spectrum of the signal to reduce the signal bandwidth and improve spectral efficiency.

### A. OVFDM SYSTEM STRUCTURE

After the data bits are mapped into symbols, they are serial-to-parallel-transformed and modulated onto different subcarriers for parallel transmission. $T$ represents the width of the OVFDM symbol. The number of subcarriers is $N$. $S_n$ $(n = 0, 1, \cdots, N-1)$ is the modulated symbols assigned to subchannels, and multiplexing waveform $rect\left(t-\frac{T}{2}\right) = 1$, $|t| \le T/2$. The OVFDM signal starting from $t = 0$ is expressed as

$$x(t) = \sum_{n=0}^{N-1} S_n rect\left(t-\frac{T}{2}\right)\exp\left(j2\pi t\frac{n}{KT}\right), \quad t\in[0,T], \tag{1}$$

where $f_n = n/T = f_0 + n\Delta f, n = 0, 1, \cdots, N-1$. Carrier spacing $\Delta f = 1/KT$ ($K$: Overlapped Multiplexing Coefficient), which makes the carriers non-orthogonal. When $K = 1$, this system is an OFDM system, otherwise it is generally referred to as an OVFDM system.

When the number of subcarriers is sufficiently large, the bandwidth requires for the OVFDM system reduces to approximately $1/K$ of the bandwidth required by the OFDM system, but it comes at the cost of orthogonality between carriers.

When the number of subcarriers $N$ is sufficiently large, the bandwidth of the OVFDM signal can be approximately $B_W \approx N\Delta f = \frac{N}{KT}$. The OVFDM signal in equation (1) is sampled by $T/N$, and we obtain (for the sake of simplicity, the rectangular function is ignored)

$$x_k = x(kT/N) = \sum_{n=0}^{N-1} S_n \exp\left(j2\pi\frac{nk}{KN}\right), \quad 0\le k\le N-1. \tag{2}$$

This is equivalent to adding $KN - N$ zeros to the data $s_n$ $(n = 0, 1, \cdots, N-1)$. And we perform IDFT operation, and take the first $N$ values in the IDFT operation result. Inverse Fast Fourier Transform (IFFT) can be used in practical applications. The processing of the entire system is shown in Fig.1.

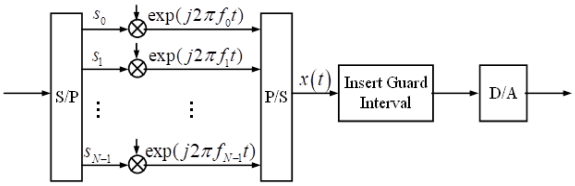


**FIGURE 1.** The schematic of OVFDM transmitter.

Since the input of the IFFT has $KN$ points and the $KN$ points of its output only take the first $N$ points, the $N_{ZP}$ point operation can be further simplified. However, compared with the minimum $N$-point IFFT operation required by the OFDM system, the minimum IFFT operation of the OVFDM system is increased.

### B. SPECTRAL EFFICIENCY

The time domain OVFDM signal is given by

$$s(t) = \frac{1}{\sqrt{T}} \sum_{k=-\infty}^{+\infty} \sum_{n=0}^{N-1} S_{k,n} g(t - kT) e^{\frac{j2\pi nt}{KT}}, \tag{3}$$

where $g(t)$ is treated as a multiplexing waveform and $T$ is the pulse duration. For the convenience of calculation, we choose rectangular waves as the multiplexed waveform here, where $rect(\cdot)$ represents a rectangular function. It is defined as

$$rect\left(\frac{t}{T}\right) = \begin{cases} 1 & -\frac{T}{2} \le t \le \frac{T}{2} \\ 0 & otherwise, \end{cases} \tag{4}$$

The frequency domain $S_k(f)$ of the $k$-th OVFDM symbol indicates

$$\begin{aligned} S_k(f) &= \mathcal{F}\left\{\frac{1}{\sqrt{T}} \sum_{n=0}^{N-1} S_{k,n} rect\left(\frac{t}{T} - k\right) e^{n\frac{j2\pi t}{KT}}\right\} \\ &= \frac{1}{\sqrt{T}} \sum_{n=0}^{N-1} \mathcal{F}\left\{rect\left(\frac{t}{T} - k\right) e^{n\frac{j2\pi t}{KT}}\right\} \\ &= \frac{1}{\sqrt{T}} \sum_{n=0}^{N-1} S_{k,n} \mathcal{F}\left\{rect\left(\frac{t}{T} - k\right)\right\} \\ &\quad \otimes \mathcal{F}\left\{1 \times e^{n\frac{j2\pi t}{KT}}\right\}, \end{aligned} \tag{5}$$

where $\mathcal{F}\{\cdot\}$ and $\otimes$ represent the Fourier transform and the convolution operation, respectively.

$$S_k(f) = \sqrt{T} \sum_{n=0}^{N-1} S_{k,n} sinc(fT) e^{j2\pi fkT} \otimes \delta\left(f - \frac{n}{KT}\right), \tag{6}$$

where $\delta(\cdot)$ represents the dirac function. Eq.(6) becomes the following

$$S_k(f) = \sqrt{T} \sum_{n=0}^{N-1} S_{k,n} sinc\left(\left(f - n\frac{1}{KT}\right)T\right) e^{j2\pi\left(f - \frac{n}{KT}\right)kT}. \tag{7}$$

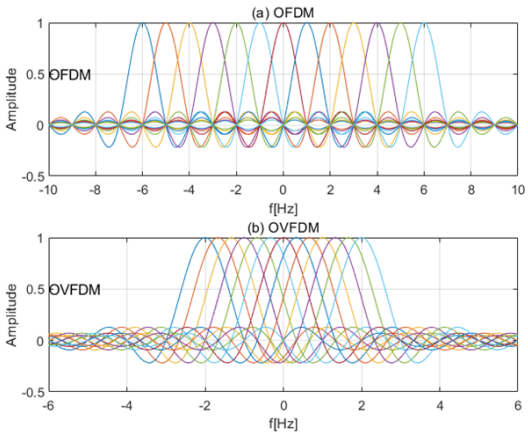


**FIGURE 2.** OFDM and OVFDM ($K = 3$) in frequency domain. $T$: 1s, subcarriers: $N = 13$.

It is apparent that the spectrum of the OVFDM symbol comprises a series of sinc functions of $1/T$ width centrally located at $n/KT$ frequencies. Fig. 2 illustrates OVFDM symbols and OFDM symbols in the frequency domain respectively. It is clear that the center of each sinc function coincides with the zero crossings of all other functions in OFDM. However, this is not the case in OVFDM scenarios with $K > 1$.

The total bandwidth $B$ of the OVFDM signal is roughly given by

$$B = (N - 1)\frac{1}{KT} + 2\frac{1}{T}, \tag{8}$$

The OVFDM spectral efficiency $\beta$ is defined as the ratio of the data bit rate $(N\log_2 M)/T$ to the signal bandwidth $B$. Therefore, $\beta$ is

$$\beta = \frac{KN\log_2 M}{(N - 1) + 2K}, \tag{9}$$

It is clear that for large $N$ and $N \gg K$, Eq. (9) can become

$$\beta = \frac{KN\log_2 M}{(N - 1) + 2K} \approx K\log_2 M. \tag{10}$$

The above formula shows that the spectral efficiency of the OVFDM system is positively correlated with the overlapping multiplexing coefficient $K$. Therefore, by increasing $K$, the spectral efficiency of the OVFDM system is significantly improved. Fig. 3 shows that how the number of subcarriers varies with the value of $K$. When the number of subcarriers is high enough, it is very close to the theoretical spectral efficiency of OVFDM.

It is notable that simulation measurements coincide with the closed formula calculations of Eq. (10) for large $N = 256$ confirming that as the normalised carriers frequency separation $K$ decreases, the noise equivalent bandwidth decreases and the OVFDM spectral gain increases proportionally.

Where $S(f)$ is the signal representation in frequency domain. The power spectral density $G(f)$ of the OVFDM signals is normalized over $\max\left\{|G(f)|^2\right\}$ and calculated

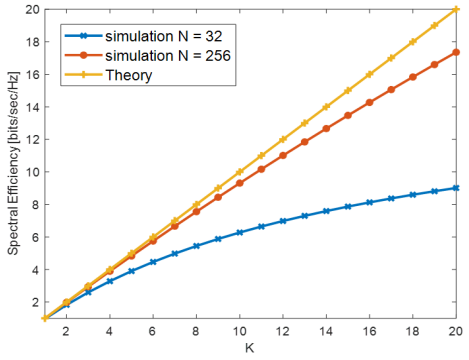


**FIGURE 3.** OVFDM spectral efficiency gain ($K = \{1 \rightarrow 20\}$ and $N = \{32, 256\}$).

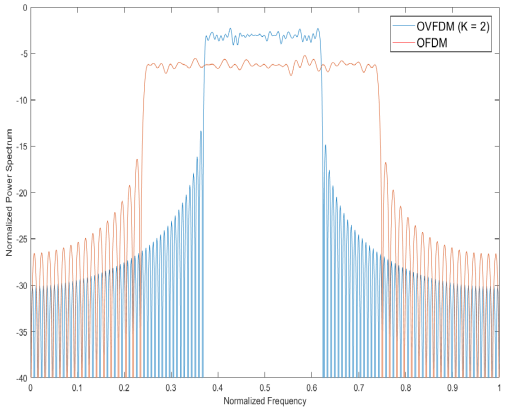


**FIGURE 4.** Power spectral density $G(f)$ for OVFDM ($K = 2$) and OFDM.

according to the following formula [16]

$$G(f) = \frac{K \int_{-\infty}^{+\infty} S^2(f)\, df}{\max\left\{\left|S^2(f)\right|\right\}}. \tag{11}$$

Fig. 4 shows the power spectral density $G(f)$ for OFDM and OVFDM with $K = 2$. It is known from Fig. 4 that the equivalent bandwidth of the OVFDM system is reduced to half that of the OFDM system, and the power spectral density of the OVFDM system is twice that of the OFDM system.

## III. THE DESIGN OF OVFDM RECEIVER UNDER RAYLEIGH CHANNEL

In this paper, our analysis of OVFDM extends from AWGN channel to fading channel. The fading channel can be interpreted as a finite impulse response filter with an impulse response of $\boldsymbol{h} = [h_0, \ldots, h_{L-1}]^T$ and its length is $L$. We consider the channel in each block to be time invariant [17].

### A. THE DTRECT FFT RECEIVER

We assume that the time-varying impulse response of the channel is $h(t, \tau)$ and the maximum delay spread is $\tau_{\max}$, and the baseband received signal is expressed as

$$y(t) = \int_0^{\tau_{\max}} h(t, \tau) x(t - \tau)\, d\tau + z(t), \tag{12}$$

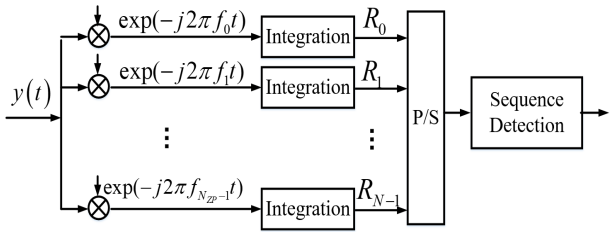


**FIGURE 5.** The schematic of the OVFDM direct FFT receiver.

where $z(t)$ is a Gaussian white noise with a mean value of zero and a bilateral power spectral density of $N_0/2$. Only the reception of one OVFDM symbol is considered below. We assume that the guard interval inserted after each data symbol is $T_g$ $(T_g > \tau_{\max})$ and the number of samples is $N_g = T_g/\Delta t = T_g N/T$. The total length of one symbol is $T_{ZP} = T + T_g$ (including $N_{ZP} = N + N_g$ samples), and the receiving end detects the transmitted data symbol according to the received signal in the interval $[0, T_{ZP}]$.

The direct FFT type receiver is similar to the receiver of the OFDM system, and the principle is expressed by the Fig. 5. After demodulating each subcarrier separately, it is integrated in one symbol period, and the obtained baseband output signal is

$$R_n = \frac{1}{T_{ZP}} \int_0^{T_{ZP}} y(t) \exp\left(-j2\pi \frac{nt}{KT}\right) dt, \quad n = 0, 1, \ldots, N-1. \tag{13}$$

If the $\Delta t = T/N$ is still sampled at the $y(t)$ sampling interval and the discrete signal sequence $\{y_0, y_1, \ldots, y_{N_{ZP}-1}\}$ is obtained, the above equation can be rewritten as

$$R_n = \frac{1}{N_{ZP}} \sum_{k=0}^{N_{ZP}-1} y_k \exp\left(-j2\pi \frac{nk}{KN}\right), \quad n = 0, 1, \cdots, N-1. \tag{14}$$

Therefore, the signal sequence $\{R_0, R_1, \cdots, R_{N-1}\}$ demodulated on the $N$ subcarriers is represented as a discrete Fourier transform (DFT) of the received signal, which is calculated by a $KN$ point DFT. The processing is as follows: firstly, zeros are added after the received signal sequence to obtain a total $KN$ point, and a $KN$ point DFT operation is performed thereon, and the first $N$ points of the operation result are taken as the received signals on each subcarrier. Similarly, since the input of the DFT has $(K-1) \times N$ zeros, and the $KN$ points of its output only take its $N$ point, the DFT operation can be further simplified.

According to Eq.(14), the received time domain sampling signal is

$$y_k = \sum_{l=0}^{L-1} h_{k,l} x_{k-l} + z_k, \quad k = 0, 1, \cdots, N_{ZP} - 1. \tag{15}$$

where $z_k$ represents the discrete additive white Gaussian noise with a mean of zero, $h_{k,l}$ represents the impulse response sample value of the $l$-th path and the $k$-th subcarrier of the

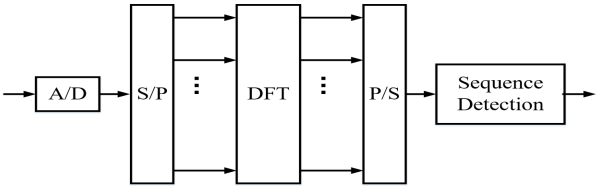


**FIGURE 6.** OVFDM direct FFT receiver baseband processing.

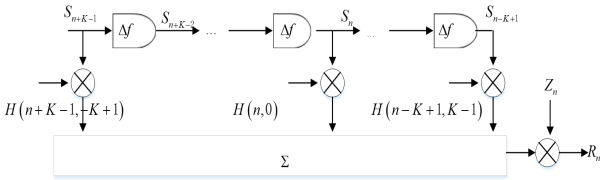


**FIGURE 7.** The signal convolutional coding model of OVFDM.

channel over time, and $L$ represents the multipath number of the discrete channel. We get

$$\begin{aligned} R_n &= \frac{1}{N_{ZP}} \sum_{k=0}^{N_{ZP}-1} \sum_{l=0}^{L-1} h_{k,l} x_{k-l} \exp\left(-j2\pi \frac{nk}{KN}\right) \\ &\quad + \frac{1}{N_{ZP}} \sum_{k=0}^{N_{ZP}-1} z_k \exp\left(-j2\pi \frac{nk}{KN}\right) \\ &= \frac{1}{N_{ZP}} \sum_{k=0}^{N_{ZP}-1} \sum_{l=0}^{L-1} h_{k,l} g_{k-l} \sum_{m=0}^{N-1} S_m \exp\left(j2\pi \frac{m(k-l)}{KN}\right) \\ &\quad \times \exp\left(-j2\pi \frac{nk}{KN}\right) + Z_n \\ &= \frac{1}{N_{ZP}} \sum_{m=0}^{N-1} S_m \sum_{l=0}^{L-1} \exp\left(-j2\pi \frac{ml}{KN}\right) \sum_{k=0}^{N_{ZP}-1} h_{k,l} g_{k-l} \\ &\quad \times \exp\left(-j2\pi \frac{(n-m)k}{KN}\right) + Z_n. \end{aligned} \tag{16}$$

where

$$Z_n = \frac{1}{N_{ZP}} \sum_{k=0}^{N_{ZP}-1} z_k \exp\left(-j2\pi \frac{nk}{KN}\right), \quad n = 0, 1, \cdots, N-1 \tag{17}$$

$Z_n$ indicates the frequency domain noise obtained after the receiver FFT operation.

If we define

$$H_l(i) = \frac{1}{N_{ZP}} \sum_{k=0}^{N_{ZP}-1} h_{k,l} g_{k-l} \exp\left(-j2\pi \frac{ik}{KN}\right), \quad i \in 0, 1, \ldots, N. \tag{18}$$

$H_l(i)$ represents the spectral spread of the $l$-path equivalent channel caused by the time-varying characteristics of the shaping filter and the channel. Similar to the received signal on each subcarrier, $H_l$ also is obtained by making a $KN$ point FFT by zero padding and then cyclically expanding. On this basis, we define

$$H(m, i) = \sum_{l=0}^{L-1} H_l(i) \exp\left(-j2\pi \frac{ml}{KN}\right), \quad m = 0, 1, \cdots, N-1. \tag{19}$$

It represents the shifted two-dimensional frequency response of the equivalent channel, which is obtained by performing a $KN$ points FFT on the $H_l$ zero-filling, and then intercepting the first $N$ points. Substituting equations (18) and (19) into equation (16), we get

$$R_n = \sum_{m=0}^{N-1} S_m H(m, n-m) + Z_n \tag{20}$$

Thus, the frequency domain received symbol sequence with one symbol period is a convolution of the transmitted symbol sequence with the equivalent channel frequency response. Due to the presence of multipath, the response of the equivalent channel on different subcarriers is different. In practice, in order to limit the interference between subcarriers, it is necessary to select a suitable shaping filter. Therefore, it can be assumed that when $|i| > K-1$, $H(m, i) = 0$, that is, the actual symbol constraint length is $2K-1$. Then there is

$$R_n = \sum_{i=-K+1}^{K-1} S_{n-i} H(n-i, i) + Z_n \tag{21}$$

Eq.(21) represents the OVFDM frequency domain received signal model, which is represented by a signal convolution model, as shown in Fig.7.

It is known from Fig.7 that the constraint length of the OVFDM is $2K-1$. For $M$-order modulation systems, the number of states in the trellis diagram is $M^{2(K-1)}$. To achieve high-spectrum OVFDM in fading channels, optimal reception with exponentially increasing computational complexity is not feasible. Therefore, it is necessary to study a new type of fast decoding algorithm to reduce the high computational complexity caused by the increase of the overlapping weight $K$.

### B. OVFDM AGAINST FREQUENCY SELECTIVITY

Inspired by OFDM, we recommend filling zeros of length $N_g \geq L$ at the end of each OVFDM block as a guard interval to avoid Inter Block Interference (IBI). We assume that $N_g < N$ is actually to ensure transmission efficiency.

As a result, we rewrite equation (22) as a vector.

$$\boldsymbol{r} = \boldsymbol{H}\boldsymbol{x} + \boldsymbol{z} \tag{22}$$

where $\boldsymbol{x} = \left[x_0, \ldots, x_{N-1}, \mathbf{0}_{1\times N_g}\right]^T$, $\boldsymbol{r} = \left[r_0, \ldots, r_{N_{ZP}-1}\right]^T$ represents the received signal vector, and $N_{ZP} = N + N_g$, $\boldsymbol{z} = \left[w_0, \ldots, w_{N_{ZP}-1}\right]^T$ represents the noise vector, and $\boldsymbol{H}$ is the $N_{ZP} \times N_{ZP}$ lower triangular Toeplitz matrix with the first column $[h_0, \ldots, h_{L-1}, 0, \ldots, 0]^T$.

Since the receiver uses the $KN$ points DFT, we reconstruct $\boldsymbol{r}$ and $\boldsymbol{x}$ in Eq. (22) into $KN \times 1$ vectors by filling zeros, ie $\boldsymbol{r} = \left[\boldsymbol{r}^T, \boldsymbol{0}_{1\times(KN-N_{ZP})}\right]^T$, $\boldsymbol{x}_0 = \left[\boldsymbol{x}^T, \boldsymbol{0}_{1\times(KN-N_{ZP})}\right]^T$. Therefore, the received signal vector in Eq. (22) has the following form

$$\boldsymbol{r}_0 = \boldsymbol{H}_0\boldsymbol{x}_0 + \boldsymbol{z}_0 \tag{23}$$

where $\boldsymbol{z}_0 = \left[\boldsymbol{z}^T, \boldsymbol{0}_{1\times(KN-N_{ZP})}\right]^T$ vector, and $\boldsymbol{H}_0$ is $KN \times KN$ lower triangular Toeplitz matrix, whose first column is

$$\boldsymbol{h}_0 = \left[\boldsymbol{h}^T, \boldsymbol{0}_{1\times(KN-L)}\right]^T \tag{24}$$

We note that the last $KN-N$ column of $H_0$ does not affect received datas $r_0$, $\boldsymbol{H}_0$ is decomposed into

$$\boldsymbol{H}_0 = \tilde{\boldsymbol{H}} - \Delta\boldsymbol{H}_0 \tag{25}$$

where $\tilde{\boldsymbol{H}}$ is the $KN \times KN$ circulant matrix of the first column $\boldsymbol{h}_0$, and $\Delta\boldsymbol{H}_0$ is the $KN \times KN$ upper triangular Toeplitz matrix of the first row $\left[\boldsymbol{0}_{1\times(KN-L+1)}, h_{L-1}, \ldots, h_1\right]$. Obviously, since $L \le N_g \le KN-N$, all non-zero terms are in the last $KN-N$ column of $\Delta\boldsymbol{H}_0$, so we can rewrite equation (23) to

$$\boldsymbol{r}_0 = \tilde{\boldsymbol{H}}x_0 + \boldsymbol{z}_0 \tag{26}$$

As shown in Fig.5, the resulting signal after performing the $KN$ points DFT in the frequency domain is given by:

$$\begin{aligned}\tilde{\boldsymbol{Y}} &= \boldsymbol{F}\tilde{\boldsymbol{H}}\boldsymbol{x}_0 + \boldsymbol{F}\boldsymbol{z}_0 \\ &= \boldsymbol{F}\tilde{\boldsymbol{H}}\boldsymbol{F}^H\boldsymbol{F}\boldsymbol{x}_0 + \tilde{\boldsymbol{Z}} \\ &= \boldsymbol{D}_{KN}\left(\tilde{\boldsymbol{h}}\right)\boldsymbol{F}\boldsymbol{x}_0 + \tilde{\boldsymbol{Z}}\end{aligned} \tag{27}$$

$\boldsymbol{F}$ denotes a $KN \times KN$ DFT matrix, $\boldsymbol{D}_{KN}\left(\tilde{\boldsymbol{h}}\right)$ denotes a $KN \times KN$ diagonal matrix, and $KN \times 1$ vector $\tilde{\boldsymbol{h}}$ on the diagonal, where the $n$-th entry of $\tilde{\boldsymbol{h}}$ represents a channel transfer function on the $n$-th subcarrier, ie

$$H_n = \sum_{l=0}^{L-1} h_l \exp\left(-\frac{j2\pi nl}{KN}\right) \tag{28}$$

As a result, ZF-FDE (frequency-domain equalizer) is implemented as

$$\hat{\boldsymbol{Y}} = \boldsymbol{D}_{KN}^{\dagger}\left(\tilde{\boldsymbol{h}}\right)\tilde{\boldsymbol{Y}} = \boldsymbol{F}\boldsymbol{x}_0 + \boldsymbol{D}_{KN}^{\dagger}\left(\tilde{\boldsymbol{h}}\right)\tilde{\boldsymbol{Z}} \tag{29}$$

$\boldsymbol{x}_0$ is the IDFT output of $\boldsymbol{s} = \left[S_0, S_1, \ldots, S_{N-1}, \boldsymbol{0}_{1\times(KN-N)}\right]^T$. Because the last $(KN-N)$ sample is replaced by zeros, it is rewrited Eq. (27) as

$$\begin{aligned}\tilde{\boldsymbol{Y}} &= \boldsymbol{D}_{KN}\left(\tilde{\boldsymbol{h}}\right)\boldsymbol{F}\boldsymbol{D}_{KN}(\boldsymbol{w})\boldsymbol{F}\boldsymbol{S}^H + \tilde{\boldsymbol{Z}} \\ &= \boldsymbol{D}_{KN}\left(\tilde{\boldsymbol{h}}\right)\boldsymbol{W}\boldsymbol{S} + \tilde{\boldsymbol{Z}}\end{aligned} \tag{30}$$

where $\boldsymbol{w} = \left[\boldsymbol{1}_{1\times N}, \boldsymbol{0}_{1\times(KN-N)}\right]^T$ and $\boldsymbol{W}$ are $KN \times KN$ cyclic Hermitian matrices, and the $(m,n)$-th entry is expressed as

$$W_{m,n} = \frac{1}{KN}\sum_{k=0}^{N-1}\exp\left(\frac{-j2\pi\,(n-m)\,k}{KN}\right) \tag{31}$$

Therefore, the received signal on the $n$-th subcarrier is

$$\tilde{Y}_n = H_nW_{n,n}S_n + \sum_{m=0,m\neq n}^{N-1} H_nW_{n,m}S_m + \tilde{Z}_n \tag{32}$$

where $\tilde{Y}_n$ represents the $n$-th entry of the $\tilde{\boldsymbol{Y}}_n$. Specifically, $\left\{W_{n,0}\right\}, n = 0, 1, \ldots, KN-1$ is the DFT of $\boldsymbol{w}$. And $W_{m,n}$, $\forall m = n$ and $\forall m \neq n$ are the weighting factors of the desired signal and ICI. Specifically, we have $\boldsymbol{W} = \boldsymbol{I}_N$ for the special case of OVFDM with $K = 1$, which is the OFDM case [18].

In order to evaluate the effect of frequency selective channel fading on OVFDM, the receiver has full data to eliminate ICI, ie

$$\begin{aligned}\tilde{Y}_{m,n} &= \tilde{Y}_m - \sum_{n=0,n\neq m}^{N-1} H_mW_{m,n}\tilde{S}_n \\ &= H_mW_{m,n}S_m + \tilde{Z}_m\end{aligned} \tag{33}$$

where $\tilde{Y}_{m,n}$ represents the received signal of the $S_m$ on the $m$-th subcarrier. In this case, the optimal decision variable $\tilde{S_m}$ on $S_m$ can be formed according to the principle of maximum ratio combining.

$$\begin{aligned}\tilde{S}_m &= \frac{\sum_{n=0}^{KN-1}\left(H_mW_{m,n}\right)^H\tilde{Y}_{m,n}}{\sum_{n=0}^{KN-1}\left|H_mW_{m,n}\right|^2} \\ &= S_m + \frac{\sum_{n=0}^{KN-1}\left(H_mW_{m,n}\right)^H\tilde{Z}_m}{\sum_{n=0}^{KN-1}\left|H_mW_{m,n}\right|^2}\end{aligned} \tag{34}$$

The variance of $\tilde{S}_m$ is $\frac{\sigma^2}{K}/\sum_{n=0}^{KN-1}\left|H_mW_{m,n}\right|^2$. The equivalent channel gain on the $m$-th subcarrier is

$$|G_m|^2 = K\sum_{n=0}^{KN-1}\left|H_mW_{m,n}\right|^2 \tag{35}$$

The effect of channel fading in the frequency domain on OVFDM is proportional to the variance of the channel gain $|G_m|^2$. The larger the variance of $\left\{|G_m|^2\right\}, m = 0, \ldots, N-1$ , the more severe the fading in the frequency domain of the equivalent channel.

*Theorem 1:* The average channel gain of OVFDM is equal to the average channel gain of OFDM in block transmission.

$$\mu = \frac{\sum_{n=0}^{KN-1}|G_n|^2}{KN} = \frac{\sum_{n=0}^{N-1}\left|H'_n\right|^2}{N} \tag{36}$$

where $H'_n = \sum_{l=0}^{L-1} h_l \exp(-((j2\pi nl)/N))$ represents the channel transfer function on the $n$-th subcarrier of OFDM.

*Proof:* See in Appendice A.

*Lemma 1:*

$$\frac{\sum_{n=0}^{KN-1}|H_n|^4}{KN} = \frac{\sum_{n=0}^{N-1}\left|H'_n\right|^4}{N} \tag{37}$$

*Proof:* See in Appendice B.

*Lemma 2:* Assume $b_n = c_n \otimes a_n$, $n = 0, 1, \ldots, KN-1$, where $\otimes$ denotes a circular convolution, and $a_n$, $b_n$, and $c_n$ are non-negative numbers that satisfy $\sum_{n=0}^{KN-1} c_n = 1$. Therefore, we have $\sum_{n=0}^{KN-1} a_n^2 \ge \sum_{n=0}^{KN-1} b_n^2$.

*Proof:* See in Appendice C.

*Theorem 2:* OVFDM is more robust to frequency selective channel fading than OFDM.

*Proof:* Theorem 2 can be characterized using the following formula:

$$\frac{\sum_{n=0}^{KN-1}\left(|G_n|^2-\mu\right)^2}{KN} \le \frac{\sum_{n=0}^{N-1}\left(\left|H_n'\right|^2-\mu\right)^2}{N} \quad (38)$$

According to Lemma 1, we can use $((\sum_{n=0}^{KN-1}|G_n|^2)/KN)-\mu^2$ and $((\sum_{n=0}^{KN-1}|H_n|^2)/KN)-\mu^2$ to rewrite the left and right terms of Eq. (35) respectively. From Eq. (34), $\left\{|G_n|^2\right\}$ is a circular convolution of $\left\{|H_n|^2\right\}$ and $\left\{K(\left|W_{0,n}\right|^2)\right\}$, and recalling Lemma 2, we conclude that Theorem 2 is correct.

As described above, the equivalent channel gain on a particular subcarrier of the OVFDM is more ''flat'' than OFDM in an actual frequency selective fading scenario.

## IV. DATA DETECTION ALGORITHM

### A. MLSD ALGORITHM AND ITS PROBLEMS

The best criterion for signal detection without prior information is maximum likelihood criterion. MLSD is a sequence detection method based on this criterion, which minimizes the block error rate of the detection output. Traditionally, MLSD of inter-symbol interference signals use Forney-type receivers or Ungerboeck-type receivers, and they both use the Viterbi algorithm (VA) to search the maximum likelihood path according to their respective Inter-Symbol Interference (ISI) model.

The OVFDM system uses the MLSD method to detect signals at the receiving end. Since channel interference is assumed to be white noise, the maximum likelihood criterion, i.e. the minimum Euclidean distance criterion [19], is

$$\hat{S}=\arg\min_{S}\sum\left|y(t)-\sum_{i=0}^{N-1}S_i\exp\left(j2\pi t\frac{i}{KN}\right)\right|^2, \quad 0\le t\le T \quad (39)$$

The Viterbi algorithm based on MLSD is the maximum likelihood algorithm in essence, but its complexity only increases exponentially with the memory length $L$ of the channel, rather than exponentially with the carrier number $N$. For this reason, it is assumed that the channel is white noise, and the input data sequence with the maximum likelihood function value in the white noise channel should be the input sequence corresponding to the path with the minimum Euclidean distance of the received signal in the Trellis graph. That is to choose the best $x(f)$, so that

$$\min_{u_n}\int_B \|V_n(f)-X_n(f)\|^2 df \quad (40)$$

where $B=\left[f_0-\frac{B}{2},f_0+\frac{B}{2}+(K-1)\Delta f\right]$ indicates the total received signal bandwidth. $X(f)$ is a symbol on the frequency domain, and $x(t)$ considers white noise $n(t)$ as a signal in the frequency domain, $V_n(f)=X_n(f)+N_n(f)$.

The physical meaning of the above formula is to find the most probable data sequence $t\in[nT_s,(n+1)T_s]$ during the $n$-th symbol duration, so that its corresponding spectrum $X_n(f)$ is closest to the spectral waveform $V_n(f)$ of the received signal (the Euclidean distance is the smallest).

### B. MAP-BASED VITERBI DECODER

In this paper, we propose a low-complexity MAP-based decoder using MLSD decoding to effectively reduce the ICI of OVFDM. Unlike the Viterbi algorithm based on the MLSD principle, we first evaluate the probability of each path and then discard the smallest possible path according to the MAP criteria to reduce the size of the search space in each step of the sequential decoding process.

#### 1) A POSTERIORI PROBABILITY OF DETECTION WITH INTERFERENCE

We consider the integrated detection of the first $P$ symbols in sequential decoding. The corresponding interference on the $k-$th subcarrier is

$$\gamma_k=\sum_{i=P}^{KN-1}W_{k,i}S_i+\hat{w}_k,\quad k=0,1,2,\ldots,P-1 \quad (41)$$

The first term on the right side of Eq. (41) represents the ICI caused by the following undetected symbol $S_i, i=P,P+1,\ldots,KN-1$. Without loss of generality, we assume that the transmitted symbol is i.i.d., and $E\left\{|S_k|^2\right\}=1$ and $E\left\{\left|S_kS_i^*\right|\right\}=0,\forall k\ne i$. Defining $\boldsymbol{\gamma}=[\gamma_0,\ldots,\gamma_{P-1}]^T$, we get $E\{\boldsymbol{\gamma}\}=\mathbf{0}_{P\times1}$, and the covariance matrix of $\boldsymbol{\gamma}$ is given by:

$$\boldsymbol{\Gamma}=\boldsymbol{W}_{12}\boldsymbol{W}_{21}+\frac{1}{K}\sigma^2\boldsymbol{D}_P\left(\left[\frac{1}{|H_0|^2}\cdots\frac{1}{|H_{P-1}|^2}\right]\right) \quad (42)$$

where $\boldsymbol{W}_{12}$ and $\boldsymbol{W}_{21}$ are $P\times(KN-P)$ upper right corner and $(KN-P)\times P$ left lower submatrix $\boldsymbol{W}$, respectively.

$$\boldsymbol{W}=\begin{bmatrix}\boldsymbol{W}_{11} & \boldsymbol{W}_{12}\\ \boldsymbol{W}_{21} & \boldsymbol{W}_{22}\end{bmatrix} \quad (43)$$

The interference term in Eq. (43) is a $P$-dimensional joint Gaussian distribution with a covariance matrix $\boldsymbol{\Gamma}$. So the posterior probability on $\hat{\boldsymbol{s}}=\left[\hat{s}_0,\ldots,\hat{s}_{P-1}\right]^T$ can be written as

$$\Pr\left\{\hat{\boldsymbol{S}}\right\}=\frac{1}{\pi^P|\boldsymbol{\Gamma}|}\exp\left(-\boldsymbol{d}^H\boldsymbol{\Gamma}^{-1}\boldsymbol{d}\right) \quad (44)$$

where

$$\boldsymbol{d}=\boldsymbol{y}-\boldsymbol{W}_{11}\hat{\boldsymbol{S}} \quad (45)$$

where $\boldsymbol{Y}=\left[\hat{Y}_0,\ldots,\hat{Y}_{P-1}\right]^T$ is the $P\times1$ subvector of $\hat{\boldsymbol{Y}}$ in Eq. (44).

After normalization, we obtain the final posterior probability of each test, ie. $p_1\ge p_2\ge\cdots\ge p_{|\mathbb{S}_P|}$, in descending order in $\mathbb{S}_P=\left\{\hat{\boldsymbol{s}}\right\}$. Specifically, $\hat{\boldsymbol{s}}_1$ indicates MAP detection, and $\hat{\boldsymbol{s}}_{|\mathbb{S}_P|}$ is the one with the smallest $\mathbb{S}_P$ possibility in the current decoding step.

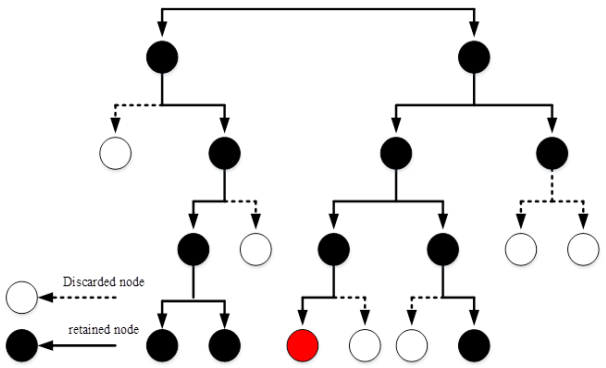


**FIGURE 8.** Tree diagram of MAP-based Viterbi decoder.

### 2) MAP – BASED VITERBI DECODING ALGORITHM

To reduce the amount of decoding scale, we take a criterion to limit the search space size of the MLSD in the $\mathbb{S}_P$ by using the minimum set. It can be known from equation (41) that the corresponding probabilities that affect $\hat{\boldsymbol{S}}$ detection are reordered with the value of $P$ increasing. It means that a subset of the tests is retained, which include MAP and sub-optimal detection. In general, a larger subset of detections produces a higher global MAP probability while requiring a higher amount of computation.

$\{p_i\}, i = 1, \ldots, |\mathbb{S}_P|$ represents the posterior probability in $\mathbb{S}_P$ in descending order. We define $\varepsilon$ as any small number between 0 and 1, and we find an integer $C \leq |\mathbb{S}_P|$.

$$\sum_{i=1}^{C} p_i \geq 1 - \varepsilon > \sum_{i=1}^{C-1} p_i \tag{46}$$

Therefore, $\mathbb{S}_P = \{s_i\}, i = 1, 2, \ldots, C$ is the smallest subset of $\mathbb{S}_P$ of a particular $\varepsilon$. In this paper, we define $\varepsilon = \lambda p_e$, where $\lambda = 0.001$.

$$f\left(p_1, \frac{E_b}{N_0}\right) = 1 - 0.1\left|\log_{10} p_1\right|^t - p_1 \times 2^{((E_b/N_0)+10)/10} \tag{47}$$

where $E_b/N_0$ represents the SNR per bit. At this time, we re-determine $\varepsilon$

$$\varepsilon = \max\left\{0.1\left|\log_{10} p_1\right|^t, \lambda p_e\right\} \tag{48}$$

where

$$t = \begin{cases} 1 & p_1 \geq 0.1 \\ 2 & p_1 < 0.1 \end{cases} \tag{49}$$

In this case, even for $0.1\left|\log_{10} p_1\right|^t \geq \lambda p_e$, we still have a fairly robust $\varepsilon \leq 0.1\left(\log_{10}|\mathbb{S}_P|^t\right)$ due to the $p_1 \geq |\mathbb{S}_P|$.

We propose a decoding algorithm based on MAP for the OVFDM system, in which the decoding process is explained by using phenogram in Fig. 8. We firstly initialize $P = 1$ and $\mathbb{S}_1 = \mathbb{Q}$, where $\mathbb{Q}$ represents the set of constellations with a base of $M$. For the sake of simplicity, we set the symbol size $Q = 2$ and $M = 1$. Then we determine the proportion of the search space by using a specific minimum set. $\varepsilon$ is in each step of sequential decoding. Based on the MAP retention/discard criteria, we retain the $C$ ML detection from the $\mathbb{S}_P$ (represented by the solid points in the $P$-th row) to reduce the computation. Finally, detection with a global MAP, i.e., $\hat{s}_1 \in \mathbb{S}_Q$, up to $P \to Q$ can be reached.

**TABLE 1.** The comparison of computational complexity.

| Algorithm | Computational complexity |
|---|---|
| MLSD (Viterbi) | $\mathcal{O}\left(N2^{2K+1}\right)$ |
| Fano | $\mathcal{O}\left(N \cdot (\log_2 M)^2\right)$ |
| Multi-Bit SSD | $\mathcal{O}\left(NK2^D + \frac{N}{D}\log N\right)(D : thelengthofSW)$ |
| MAP-based Viterbi | $\mathcal{O}\left(\frac{M(M+1)(2M^2+4M+2NCM+7NC-2NC-1)}{6}\right)$ |

**TABLE 2.** COST207 RA channel model.

| Tap | Delay,(us) | Power |
|---|---|---|
| 1 | 0.0 | 0.602 |
| 2 | 0.1 | 0.241 |
| 3 | 0.2 | 0.096 |
| 4 | 0.3 | 0.036 |
| 5 | 0.4 | 0.018 |
| 6 | 0.5 | 0.006 |

### 3) DECODING ALGORITHM AND COMPLEXITY ANALYSIS

We show the decoding complexity of the MAP-based Viterbi decoding algorithm and compare it with the Viterbi decoding algorithm, Fano algorithm, and Multi-Bit SSD algorithm. Table 1 shows a comparison of the computational complexity of the proposed detection algorithm.

## V. SIMULATION RESULTS

We set the OVFDM system to have 128 subcarriers with perfect synchronization. We consider the use of BPSK modulation, and the multiplexing waveform uses a rectangular wave. Generally, compared with OFDM, OVFDM system saves $((K-1)N + 1 - K)/KT$ spectrum, that is, for the available bandwidth $B = 10$ MHz, OVFDM requires only about $(10/K)$ MHz of actual bandwidth. In this paper, the typical rural area of COST207 RA channel model [20] ( $h(n) = 0.602(n) + 0.241(n-1) + 0.096(n-2) + 0.036(n-3) + 0.018(n-4) + 0.006(n-5)$ is given in Tab. 2) is used as the fading environment. To facilitate subsequent work, we assume that the channel state information is known and the channel coefficient is constant [21].

### A. PERFORMANCE EVALUATION

We evaluate the BER of the new decoder on OVFDM through the AWGN channel. As shown in Fig.9, the performance difference of OVFDM for OFDM of the same constellation is not large, but its spectral efficiency is doubled. Under the COST207 RA channel model, OVFDM achieves similar BER for OFDM under low SNR conditions. With the increase of

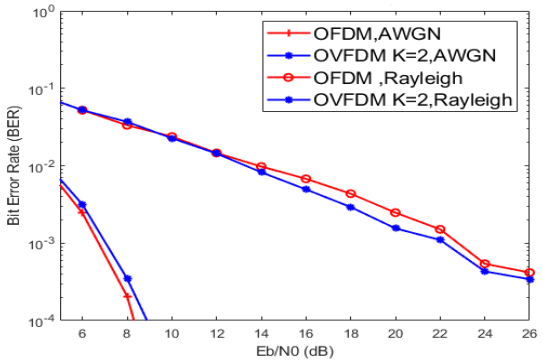


**FIGURE 9.** The BER performance comparison of OVFDM ($K = 2$) and OFDM.

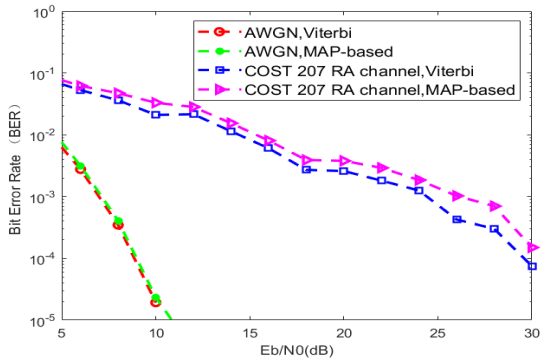


**FIGURE 11.** The BER performance of the MAP-based Viterbi algorithm and Viterbi algorithm for OVFDM ($K = 2$) system in AWGM channel and COST207 RA channel model.

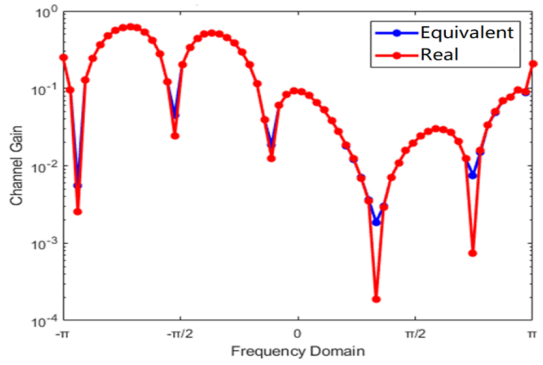


**FIGURE 10.** Channel frequency response.

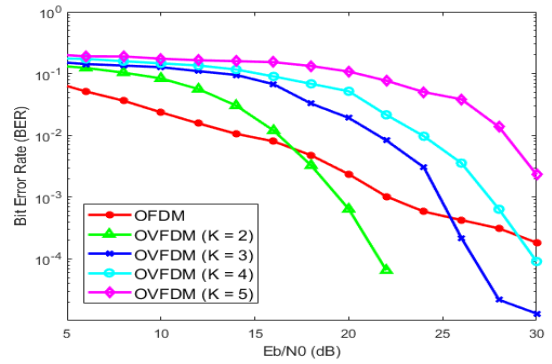


**FIGURE 12.** The decoding performance of OVFDM for various $K$ values.

SNR, the BER performance of OVFDM is gradually better than OFDM under the same conditions.It shows that the OVFDM ($K = 2$) system provides twice the spectral efficiency of the OFDM system and achieves BER performance similar to OFDM. Analyzing the reasons, the proposed equalization and detection of OVFDM can benefit from channel frequency diversity, which improves its anti-fading performance in the actual frequency selective fading environment.

In order to verify the advantages of OVFDM over the fading scenario, we compare the difference between $|G_k|^2$ and $|H_k|^2$. From Fig. 10, OVFDM is quite robust. It can be seen from the comparison that the equivalent channel response help OVFDM resist the interference caused by the fading channel, which makes the OVFDM decoding effect better. The simulation results prove OVFDM with ZP-OVFDM structure applicable to fading channels.

Next, we use the Viterbi decoding algorithm as a reference to verify the proposed decoding algorithm. Because Viterbi decoding has the best ML performance, we use it here as a benchmark for decoding algorithms to compare the performance of the algorithm proposed in this article. To get closer to the real situation, we consider the COST207 RA channel model. It shows the similar decoding performance of the proposed decoding algorithm and Viterbi algorithm for OVFDM ($K = 2$) system in Fig. 11.

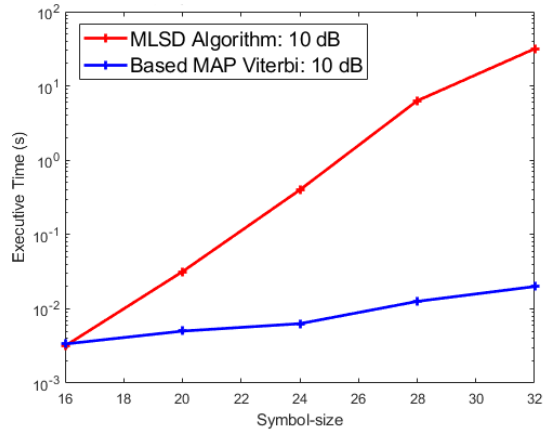


**FIGURE 13.** The average execution time with various symbol sizes $N$.

We find from Fig. 12 that OVFDM with ZP-OVFDM has better BER performance than OFDM under high signal-to-noise ratio when $K = 4$. When $K = 5$, the BER performance of OVFDM is slightly worse than that of OFDM. The multiplexing waveforms in the frequency domain are too dense, which exceed the performance range of the data detection algorithm. The simulation results prove that the proposed decoding algorithm has excellent robustness against multipath fading on multipath fading channel.

### B. THE COMPLEXITY ANALYSIS

As shown in Fig. 13, there is little difference between the execution time of MLSD algorithm and MAP-based Viterbi algorithm in the case of a short symbol length. However, with the increase of the symbol length, the decoding time of MLSD algorithm and MAP-based Viterbi algorithm is much different. Meanwhile, we see that the calculation time of MAP-based Viterbi decoding algorithm does not increase significantly with the size of the symbol.

## VI. CONCLUSION

This paper focuses on channel equalization and data detection of OVFDM systems on frequency-selective fading channels. First, the system model and spectrum efficiency of OVFDM are proposed. Then mathematical analysis is used to derive the transmission and reception process of the OVFDM system under the frequency-selective fading channel, and a ZP-OVFDM architecture is proposed and verified that the structure can benefit from the frequency diversity of channel response. Next, this paper proposes a MAP-based Viterbi decoding algorithm, and further provides a minimum set of retention / discarding criteria to reduce the size of the search space in MLSD detection, which reduces the calculation complexity. Compared with the MLSD algorithm has better performance, the proposed detection scheme has better performance, and the required calculation amount is much lower. Therefore, compared with OFDM, OVFDM systems with the proposed equalization and detection algorithm have the potential to improve spectral efficiency dramatically.

## APENDIXES

## APPENDIX A
## PROOF OF THEOREM 1

According to Eq.(32), Eq.(36) and Parseval theorem [22], we have

$$\begin{aligned}\frac{\sum_{k=0}^{N-1}|G_k|^2}{KN} &= \frac{K\sum_{k=0}^{N-1}\sum_{n=0}^{N-1}\left|H_nW_{n,k}\right|^2}{KN}\\ &= \frac{K\sum_{n=0}^{N-1}|H_n|^2\sum_{k=0}^{N-1}\left|W_{n,k}\right|^2}{KN}\\ &= \sum_{l=0}^{L-1}|h_l|^2\\ &= \frac{\sum_{k=0}^{N-1}\left|H'_k\right|^2}{N}\end{aligned} \tag{50}$$

This leads to Eq.(37) and completes the proof of the theorem.

## APPENDIX B
## LEMMA PROOF 1

We have $h_l{}' = h_l^* h_l$, and the length of $h_l{}'$ is $2L-1 < N$. According to the convolution theorem, we have

$$H'^2_k = \sum_{l=0}^{L-1} h'_l \exp\left(-\frac{j2\pi kl}{N}\right), \tag{51}$$

And

$$H_k^2 = \sum_{l=0}^{L-1} h'_l \exp\left(-\frac{j2\pi kl}{KN}\right), \tag{52}$$

In turn, according to the Parseval theorem, we have $\sum_{k=0}^{Q-1}\left|H'^2_k\right|^2 = \sum_{l=0}^{L-1}\left|h'\right|_l^2 = \sum_{k=0}^{N-1}\left|H_k^2\right|^2$,in the light of Parseval's theorem. This completes the proof of Lemma 1.

## APPENDIX C
## LEMMA PROOF 2

Since $b_n$ is a circular convolution of $a_n$ and $c_n$, we have

$$\begin{aligned}\sum_{n=0}^{N-1} b_n^2 &= 2\sum_{i_1=0}^{N-1}\sum_{j_1\neq i_1}\sum_{i_2=0}^{N-1}\sum_{j_2\neq i_2} c_{i_1}c_{j_1}a_{i_2}a_{j_2}\\ &\quad+\left(\sum_{n_1=0}^{N-1}c_{n_1}^2\right)\left(\sum_{n=0}^{N-1}a_n^2\right)\\ &= 2\sum_{i_1=0}^{N-1}\sum_{j_1\neq i_1}\left(c_{i_1}c_{j_1}\right)\sum_{i_2=0}^{N-1}\sum_{j_2\neq i_2}\left(a_{i_2}a_{j_2}\right)\\ &\quad+\left(\sum_{n_1=0}^{N-1}c_{n_1}^2\right)\left(\sum_{n=0}^{N-1}a_n^2\right)\\ &\leq \left(\sum_{n_1=0}^{N-1}c_{n_1}^2+2\sum_{i_1=0}^{N-1}\sum_{j_1\neq i_1}\sum_{i_1=0}^{N-1}\sum_{j_1\neq i_1}\left(c_{i_1}c_{j_1}\right)\right)\\ &\quad\times\left(\sum_{n=0}^{N-1}a_n^2\right)\\ &= \left(\sum_{n_1=0}^{N-1}c_{n_1}\right)^2\left(\sum_{n=0}^{N-1}a_n^2\right)\\ &= \sum_{n=0}^{N-1}a_n^2\end{aligned} \tag{53}$$

Obviously, the equation is true if and only if $a_i = a_j, \forall i \neq j$.

## REFERENCES


[1] H. Jiang, D. Li, and W. Li, "Performance analysis of overlapped multiplexing techniques," in *Proc. 3rd Int. Workshop Signal Design Appl. Commun.*, Sep. 2007, pp. 233–237.

[2] D. Li, "A novel high spectral efficiency waveform coding-OVFDM," *China Commun.*, vol. 12, no. 2, pp. 61–73, Feb. 2015.

[3] Q. Bi, "Ten trends in the cellular industry and an outlook on 6G," *IEEE Commun. Mag.*, vol. 57, no. 12, pp. 31–36, Dec. 2019.

[4] M. Katz, P. Pirinen, and H. Posti, "Towards 6G: Getting ready for the next decade," in *Proc. 16th Int. Symp. Wireless Commun. Syst. (ISWCS)*, Aug. 2019, pp. 714–718.

[5] S. Weinstein and P. Ebert, "Data transmission by frequency-division multiplexing using the discrete Fourier transform," *IEEE Trans. Commun. Technol.*, vol. 19, no. 5, pp. 628–634, Oct. 1971.

[6] W. Jian, Y. Xun, Z. Xi-lin, and D. Li, "The prefix design and performance analysis of DFT-based overlapped frequency division multiplexing (OvFDM-DFT) system," in *Proc. 3rd Int. Workshop Signal Design Appl. Commun.*, Sep. 2007, pp. 361–364.

[7] D. H. Bailey and P. N. Swarztrauber, "The fractional Fourier transform and applications," *SIAM Rev.*, vol. 33, no. 3, pp. 389–404, 1991.

[8] B. Muquet, Z. Wang, G. B. Giannakis, M. de Courville, and P. Duhamel, "Cyclic prefixing or zero padding for wireless multicarrier transmissions?" *IEEE Trans. Commun.*, vol. 50, no. 12, pp. 2136–2148, Dec. 2002.
[9] Y. Ding, T. N. Davidson, Z.-Q. Luo, and K. M. Wong, "Minimum ber block precoders for zero-forcing equalization," *IEEE Trans. Signal Process.*, vol. 51, no. 9, pp. 2410–2423, Sep. 2003.
[10] J. Wang, J. Song, Z.-X. Yang, L. Yang, and J. Wang, "Frames theoretic analysis of zero-padding OFDM over deep fading wireless channels," *IEEE Trans. Broadcast.*, vol. 52, no. 2, pp. 252–260, Jun. 2006.
[11] D. Zhao, D. Li, and X. Jin, "Sphere-decoding of OvTDM," in *Proc. 3rd Int. Workshop Signal Design Appl. Commun.*, Sep. 2007, pp. 22–25.
[12] B. Hassibi and H. Vikalo, "On the sphere-decoding algorithm I. Expected complexity," *IEEE Trans. Signal Process.*, vol. 53, no. 8, pp. 2806–2818, Aug. 2005.
[13] H. Zhang, Y. Chen, D. Li, and Y. Wang, "Low-complexity sliding window block decoding using bit-flipping for OVFDM systems," *IEEE Access*, vol. 5, pp. 25171–25180, 2017.
[14] P. Lin, Y. Wang, and D. Li, "Multi-bit sliding stack decoding algorithm for OVXDM," *China Commun.*, vol. 15, no. 4, pp. 179–191, Apr. 2018.
[15] P. Lin, Y. Wang, and D. Li, "Low-complexity multiple-signal joint decoding for overlapped x domain multiplexing signalling," *IET Commun.*, vol. 12, no. 11, pp. 1273–1282, Jul. 2018.
[16] C. A. Janet Rutledge Bruce Carlson and B. Paul Crilly, *Communication Systems: An Introductyion to Signal and Noise in Communication Systems*, 4th ed. New York, NY, USA: McGraw-Hill, 2002.
[17] D. R. Morgan, "Analysis and realization of an exponentially-decaying impulse response model for frequency-selective fading channels," *IEEE Signal Process. Lett.*, vol. 15, pp. 441–444, 2008.
[18] Z. Chen, X. Xu, and X. Dai, "A low-complexity transceiver scheme based on minimum Euclidean distance criterion," in *Proc. 6th Int. Conf. Wireless Commun. Signal Process. (WCSP)*, Oct. 2014, pp. 1–6.
[19] B. Yu, S. Zhang, X. Dai, and H. Zhang, "Iterative decoder for coded SEFDM systems," in *Proc. IEEE 17th Int. Conf. Commun. Technol. (ICCT)*, Chengdu, China, Oct. 2017, p. 145.
[20] A. Bishnu and V. Bhatia, "On performance analysis of IEEE 802.22 (PHY) for COST-207 channel models," in *Proc. IEEE Conf. Standards for Commun. Netw. (CSCN)*, Oct. 2015, pp. 229–234.
[21] H. Ghannam and I. Darwazeh, "Robust channel estimation methods for spectrally efficient FDM systems," in *Proc. IEEE 87th Veh. Technol. Conf. (VTC Spring)*, Jun. 2018, pp. 1–6.
[22] S. S. Kelkar, L. L. Grigsby, and J. Langsner, "An extension of Parseval's theorem and its use in calculating transient energy in the frequency domain," *IEEE Trans. Ind. Electron.*, vols. IE–30, no. 1, pp. 42–45, Feb. 1983.

**YUE HU** (Graduate Student Member, IEEE) received the B.S. degree in communication engineering from Hebei Normal University, China, in 2014, and the M.S. degree in communication and information system from the North China University of Technology, Beijing, China, in 2017. He is currently pursuing the Ph.D. degree in information and communication engineering with the Beijing University of Posts and Telecommunications. His current research interests include wireless communications and networks, with an emphasis on information and coding theory.

**YAFENG WANG** (Senior Member, IEEE) received the B.Sc. degree from the Beijing University of Posts and Telecommunications, in 1997, the M.Eng. degree from the University of Electronic Science and Technology of China, in 2000, and the Ph.D. degree from the Baoji University of Arts and Science, in 2003. He is currently a Professor of electronic engineering with the School of Information and Telecommunications, Beijing University of Posts and Telecommunications. He leads the Broadband Mobile Communication Engineering Laboratory, which is one of Zhongguancun Science Park Open Labs. In 2008, he was a Visiting Scholar with the Faculty of Engineering and Surveying, University of Southern Queensland, Australia. He has published over 100 articles in peer-reviewed journal and conference papers. His research interests include wireless communications and information theory.

**HAOCHENG WANG** received the bachelor's degree in applied physics from the Beijing University of Posts and Telecommunications, in 2018, where he is currently pursuing the M.Tech. degree in communication and information engineering with the School of Information and Communication Engineering.